Structuring effect of some salts on glycerol carbonate: A near-infrared spectroscopy, small- and wide-angle X-ray scattering study

Duccio Tatini [a], Ilaria Clemente [a], Moira Ambrosi [a], Sandra Ristori [a], Barry W. Ninham [b], Pierandrea Lo Nostro [a,c,*]

[a] *Department of Chemistry "Ugo Schiff" and CSGI, University of Florence, 50019 Sesto Fiorentino (Firenze), Italy*
[b] *Department of Applied Mathematics, Research School of Physical Sciences and Engineering, Australian National University, Canberra, ACT 0200, Australia*
[c] *Enzo Ferroni Foundation, 50019 Sesto Fiorentino (Firenze), Italy*

ARTICLE INFO

ABSTRACT

Alkylene carbonates such as ethylene, glycerol and propylene carbonates offer a valuable tool for the investigation of intermolecular interactions in polar non-aqueous liquids. Their physico-chemical properties suggest the presence of a strong structure that mainly depends on hydrogen bonds. The addition of salts bearing basic anions such as fluoride, carbonate and phosphate leads to the formation of free ions and ion pairs that are well accommodated in the solvent structure.

In this work near infrared and attenuated total reflection Fourier-transform infrared spectroscopy, small- and wide-angle X-ray scattering were carried out on pure glycerol carbonate and on its solutions of saturated KF, K_2CO_3 and K_3PO_4 in order to probe the structure of the solvent. Linear and cyclic oligomeric clusters produced by the association of the liquid molecules are proposed. The different effectiveness of the studied anions in enhancing the internal arrangement of the liquid can be explained in terms of polarizability (i.e. of the delocalization of their charge), different basicity and hydrogen bonding (HB) accepting capacity and geometry of the anions.

© 2021 Elsevier B.V. All rights reserved.

1. Introduction

Glycerol carbonate (GC) is an interesting liquid for several reasons. It has applications in a range of fields, from green chemistry (e.g., in the production of biodiesel) to industrial processes, such as catalysis, polymer synthesis, hydrocarbon separation and membrane preparation [1–11].

But also from the scientific point of view this polar non-aqueous liquid is considered an important tool for the understanding of intermolecular interactions.

As a pure liquid, GC shows some interesting features (see Table 1 in Ref. [12]). It has a very high density (1.3969 g/mL), dielectric constant (109.7), dipole moment (5.05 D) [13], viscosity (85.4 cP) [14], polarizability (9.3 $Å^3$) [15], and heat capacity (213.6 J/mol·K)

[16], and large vaporization entropy $\Delta_{vap} S$ of 125 J/mol·K (for water $\Delta_{vap}S$ is 109 J/mol·K) with a significant deviation from the Trouton's rule. It also undergoes a glass transition at −70.8 °C rather than crystallizing [17–19,12].

These properties reflect the strong highly cooperative van der Waals interactions that hold GC molecules together. Moreover, GC is a chiral molecule, in fact the ring carbon that bears the –CH_2-OH group is asymmetric.

Prompted by its structural features (see Fig. 1) and physico-chemical properties we suggested that pure GC is associated in the liquid state, stabilized by an intermolecular hydrogen bonding (HB) between the terminal –OH and C = O groups [19]. How the molecules interact in the 3D space is a question shared with water, alcohols and other liquids and is still open. Different options can be proposed, including those depicted in Fig. 2 (ribbon) and 3 (dimer). In the ribbon arrangement the dipoles are aligned in the same direction and every –OH is bound to the next carbonyl group through a HB. In the latter structure two molecules form an independent *dimer* through two HBs but the dipoles point in opposite directions. Such arrangements could contribute to giant dipole fluctuation forces with charged solutes [20]. Dynamic multiple

Table 1

Values of the molar mass (*M*, in g·mol^{-1}), density at 25° C (ρ, in g·cm^{-3}), molar volume (*V*, in cm^3·mol^{-1}), enthalpy of vaporization (Δ$_{vap}$*H*^{0} in kJ·mol^{-1}), solubility parameter (δ in MPa$^{1/2}$), fraction of free volume (*Φ*), fluidity (*φ*, in mPa^{-1}·s^{-1}), Trouton's constant (Δ$_{vap}$*S/R*) and Kirkwood's parameter (*g*) for ethylene carbonate (EC), propylene carbonate (PC) and glycerol carbonate (GC) and water.

	M	ρ	*V*	Δ$_{vap}$*H*^{0}	δ	*Φ*	*φ*	Δ$_{vap}$*S/R*	*g*
EC	88.06	1.321	66.7	59.6[a]	29.2	0.167	0.526	13.8	1.50
PC	102.09	1.200	85.1	55.2[b]	24.9	0.181	0.395	12.9	1.23[c]
GC	118.09	1.3969	84.5	85.4[d]	31.3	0.106	0.012	16.4	2.90
Water	18.02	0.997	18.1	44.0	48.0	0.092	1.123	13.1[e]	2.57[e]

a: from Ref. [49].
b: from Ref. [50].
c: from Ref. [51].
d: from Ref. [52].
e: from Ref. [53].

membered rings like those that form in water may also be possible [21].

Other patterns are possible, for example oligomeric rings. In all these clusters a HB is formed between the carbonyl and the hydroxyl groups of two adjacent molecules. However, other associated structures are feasible, where the HB is established between two –OH residues of two GC molecules. Fig. 4 shows a couple of examples of closed and open oligomers where the single GC molecules are held together by hydrogen bonds.

The occurrence of thixotropy in GC was detected from the flow curve of the pure liquid under increasing stress and then relaxation [19]. The hysteresis of the two curves is large. The phenomenon was interpreted as the effect of the shear stress on the strong structure in the liquid that is progressively weakened and then recovers when the mechanical perturbation is stopped.

While the molecules' alignment in the liquid state is the object of computational studies [22,23], here we are interested in investigating the spectroscopic and structural properties of liquid GC that reflect and can provide useful information on the intermolecular forces, especially hydrogen bonding.

Previous works reported on the solubility of some strong electrolytes in glycerol carbonate [19] and on the modification of several physico-chemical properties of the liquid (e.g. rheology, conductivity, NMR chemical shift, ATR spectra, and thermal behavior) upon the addition of a number of different potassium salts to GC [12]. The results suggested that some salts, i.e. potassium fluoride, carbonate and phosphate - where the anion acts as a HB acceptor - apparently strengthen the liquid structure by directly participating in the intermolecular hydrogen bonding [12,23].

These previous works opened interesting questions and prompted for a detailed investigation on pure GC and its solutions. Here we performed near-infrared spectroscopy (NIR), small-angle
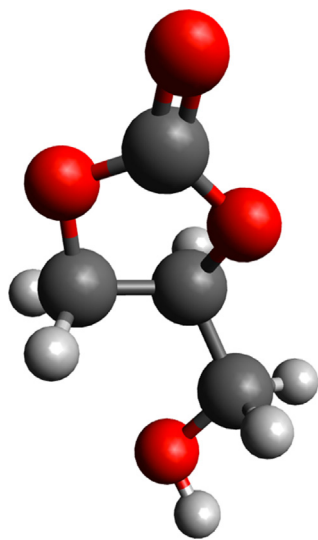
**Fig. 1.** Chemical structure of glycerol carbonate. The geometry was optimized with the Avogadro software (v.1.2.0). Dark grey, red and light grey spheres represent carbon, oxygen and hydrogen atoms, respectively.
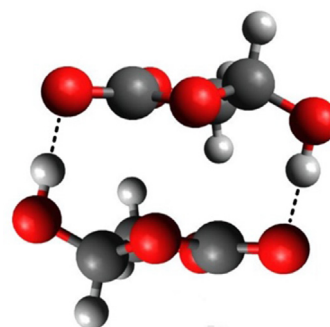
Fig. 3. Structure of a dimer from two GC molecules. The dotted segments represent hydrogen bonds.
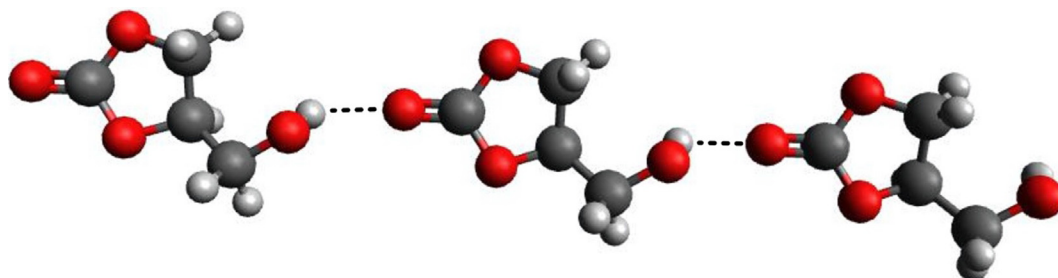
Fig. 2. Ribbon alignment of GC molecules. The dotted segments represent hydrogen bonds.
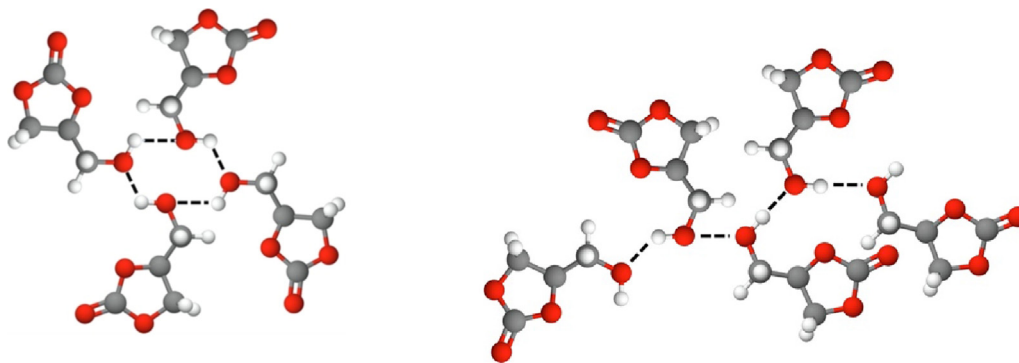
Fig. 4. Ring (left) and open (right) structures of oligomers from GC molecules stabilized by HB (dotted segments) between hydroxyl groups. Grey, red and white spheres represent carbon, oxygen and hydrogen atoms, respectively.

X-ray scattering (SAXS) and wide-angle X-ray scattering (WAXS) experiments on pure GC and in the presence of KF, K_2CO_3 and K_3PO_4 at high concentration (or at saturation) to shed light on the changes in the GC molecules induced by salts whose ions are capable of fitting in the HB network of the pure liquid.

The analysis of NIR spectra is a helpful tool for this purpose and has been used for the investigation of molecular association in pure water, salt solutions, and biological systems [24–28], the self-association of alcohols and surfactants via hydrogen bonds [29–33], and the study of structure and dynamics of water molecules in different matrixes, polymers, [34] food [35] and pharmaceuticals [36].

SAXS is a very suitable technique for the study of molecular association in many different systems, such as ordered liquids, polymers, lipid layers, nanoparticles and biomolecules [37–40]. In particular, when used in association to WAXS, SAXS allows multi-scale characterization of the spatial arrangement of atoms and molecules from Å to nm- and to μm-scales [41,42]. As with infrared spectroscopy, and at variance with microscopy, the data obtained from scattering methods are averaged on the macroscopic sample under study and therefore IR and SAXS/WAXS can be used in combination to obtain remarkable insight on structured fluids.

The results presented in this work show that anions exhibiting a strong basic nature such as F^-, CO_3^{2-} and PO_4^{3-} are able to intercalate among GC molecules and for new HBs which have a significant effect on the structure of the pure liquid.

2. Materials and methods

2.1. Materials

Glycerol carbonate or 4-(Hydroxymethyl)-1,3-dioxolan-2-one (≥90.0%, CAS Nr. 931-40-8), potassium fluoride (≥99.5%), potassium carbonate (≥99.0%) and potassium phosphate (≥98.0%) were purchased from Sigma-Aldrich (Milan, Italy). The salts were purified, dried and stored under vacuum, according to the standard procedures [12]. Glycerol carbonate was used as received and kept under inert atmosphere to avoid water contamination.

2.2. Near-Infrared and FTIR spectroscopy

NIR spectra were acquired in the wavenumber range 8000–4000 cm^{-1}, with a Nexus 870-FTIR (Thermo-Nicolet) and a FT-IR Continuum microscope in diffuse reflectance mode (beam splitter: CaF_2; detector: InGaAs) with a resolution of 8 cm^{-1} and coadding 256 scans. A Linkam THMS600 stage was used to control the sample temperature in the range 0 – 90 °C. A constant dry nitrogen flux

was applied on the external part of the Linkam window to prevent the condensation of ambient moisture. The deconvolution of the experimental spectra was performed by means of Igor Pro 6.36 using a combination of Gaussian distributions.

Attenuated total reflection Fourier-transform infrared spectroscopy (ATR-FTIR) spectra were acquired using a Thermo Nicolet Nexus 870 FT-IR spectrophotometer, equipped with a liquid nitrogen cooled MCT (mercury-cadmium-telluride) detector, by averaging on 128 scans at a resolution of 2 cm^{-1}. The spectra were acquired in the range 4000–500 cm^{-1}. The spectra were processed in order to remove the contribution of the atmospheric CO_2 and subtract the background (that was recorded before each experiment). Since GC is only sparingly soluble in deuterated chloroform, a couple of drops of GC were shaken in 1 mL of $CDCl_3$ and left to rest for 1 h before placing some drops of the solvent between two crystal windows.

2.3. Small angle X-Ray scattering (SAXS) and Wide-Angle X-ray scattering (WAXS)

SAXS experiments were performed at the high-brilliance ID02 beamline of the European Synchrotron Radiation Facility (Grenoble, France). The wavelength of the incoming beam was 1 Å, and the sample-to-detector distances were 0.8, 10, and 31 m, which covered a wide total q range, i.e. $3 \cdot 10^{-4}$ to 0.75 $Å^{-1}$ ($q = (4\pi/\lambda) \sin\theta$, where 2θ is the scattering angle and q the momentum transfer) [43,44]. The sample holder was a flow-through capillary of 2 mm diameter, which was kept in place during all measurements to optimize background subtraction. The 2D SAXS patterns initially recorded were azimuthally averaged to obtain 1D patterns and normalized to the absolute scale using a standard procedure. The resulting 1D patterns from the different configurations were merged and the background was subtracted. The curves fitting was performed by using the SasView 4.2 package.

WAXS experiments were carried out at room temperature on a Bruker D8-Da Vinci diffractometer (Cu Kα radiation, 40 kV × 40 mA), equipped with a Bruker LinXEYE detector, in a scanning range 2θ between 5 and 120° (that converting from radiants to degrees and extracting q, corresponds to 0.35–8.53 $Å^{-1}$), with 0.03° increments of 2θ and a time per single step of 192 s.

3. Results and discussion

3.1. General remarks

As we anticipated in the Introduction, the properties of glycerol carbonate reflect the strength and ordering induced by intermolec-

ular interactions in the condensed phase, i.e. hydrogen bonding and van der Waals interactions [45].

In fact apparently they reveal the existence of a dense structure in the liquid that let us envisage the presence of dimers and/or higher supramolecular associates. The existence of molecular clusters that form the structure of associated liquids is a very interesting topic since it affects the physico-chemical behavior of the pure liquid and of its mixtures [46].

There are also other parameters that describe, at least at a semi-quantitative level, the structuredness of a solvent, and that can be calculated from its experimental properties [47]. Among these:

i) The *stiffness* of a liquid structure, i.e. the resistance of the structure to molecular motion, quantifies the energy required to pull the molecules apart and create a cavity in the bulk and can be expressed as the difference between the cohesive energy density (the square of the Hildebrand solubility parameter δ) and the internal pressure P_i [48]:

$$\delta^2 - P_i = \frac{\Delta_{vap}H^0 - RT}{V} - \frac{T\alpha}{\kappa} + p \tag{1}$$

$\Delta_{vap}H^0$, V, R, T, α, κ and p are the standard evaporation enthalpy change, the molar volume (calculated from the molar mass and the density), the universal gas constant, the absolute temperature, the isobaric expansibility, the isothermal compressibility and the vapor pressure, respectively. For water the value of δ^2-P_i is 2129 MPa at 298.15 K. The values of $\Delta_{vap}H^0$, V and δ are reported in Table 1 for EC, PC, GC and water for comparison.

The cohesive energy density for GC is higher than that of EC and PC, suggesting a great stiffness for GC. For comparison we recall that δ is about 26.5 and 33 MPa$^{1/2}$ for ethanol and ethylene glycol, respectively.

ii) The *openness* depends mainly on the free volume of the solvent, i.e. the difference between its bulk molar volume and the intrinsic molar volume [53]. The latter can be estimated from either the van der Waals volume or from the McGowan intrinsic volume (V_X). We used the McGowan value because it takes into account the excluded volume surrounding a certain molecule, where another particle cannot penetrate. The calculation of V_X is straightforward from the molecular formula of the liquid [54]. The openness can be evaluated from the fraction of free volume, $\Phi = 1-(V_X/V)$, where V is the molar volume of the liquid. Table 1 lists the values of Φ for EC, PC, GC and water for comparison at 298 K. The data show that GC is very close-packed, almost as water, while EC and PC are more open. Just for comparison, other polar liquids such as 1,2-ethanediol, glycerol, and formamide possess Φ < 0.1. The openness of a liquid can also be assessed through its fluidity, which is the reciprocal of the dynamic viscosity, $\varphi = \eta^{-1}$. However the openness and the fluidity are less correlated [53]. Table 1 lists the values of φ for EC, PC and GC at 298 K. The data show that EC is almost 50 times more "open" than GC.

iii) The *ordering* reflects the difference between the molar entropy of the liquid and that of the same substance in its ideal gas state. There are different ways to estimate such entropy difference. The dimensionless Trouton's constant, $\Delta_{vap}S/R$, that for ordered liquids is greater than 12 (13.15 for water), is about 16.4 for GC, 13.8 for EC and 12.9 for PC (see Table 1). For solvents that are considered to be unstructured and non-associated, e.g. for dichloromethane, it falls between 10.5 and 11 [55]. Other ways to quantify the order in a liquid are: (a) the vaporization entropy deficit of the solvent relative to its vapor and compared with a completely unordered liquid (the "alkane homologue") $\Delta\Delta_{vap}S$, that takes into account also the possible association of molecules in the vapor state, and (b) the thermal energy per unit volume and relative to the corresponding amount for the vapor in the ideal state $\Delta C_p/V$ [51,53]. Unfortunately some of the properties needed

to estimate $\Delta\Delta_{vap}S$ and $\Delta C_p/V$ are not known for alkylene carbonates, yet.

iv) Another quantification for a polar solvent structure derives from the Kirkwood's dipole angular correlation parameter, g [47]:

$$g = \frac{9k_B\varepsilon_0 VT}{N_A\mu^2} \frac{(\varepsilon - 1.1n_D^2)(2\varepsilon + 1.1n_D^2)}{\varepsilon(2 + 1.1n_D^2)^2} \tag{2}$$

where k_B, ε_0, N_A, V, T, μ, ε and n_D are the Boltzmann constant, the vacuum permittivity, the Avogadro number, the molar volume, the absolute temperature, the dipole moment, the dielectric constant and the refractive index at the sodium D line, respectively. This parameter measures the deviation of the solvent's dielectric constant ε from the value expected for a liquid with the same dipole moment and polarizability but where the dipoles are not correlated by any liquid's structure. Thus, for unstructured solvents g = 1, whilst structured solvents generally have g greater than 1. By the way, for cyclic carbonates we calculated 2.90 for GC, 1.05 for PC, and 1.50 for EC. However, if the dipoles are not aligned in a parallel way, but in an antiparallel fashion, then g < 1 even when the solvent is strongly ordered [47]. This is a remarkable point, as the value of g significantly differs from unity for GC.

These structure-related values for GC apparently suggest that this liquid is associated and forms transient structures such as dimers or hierarchically higher clusters with non-null overall dipole moment.

3.2. Infrared spectroscopy

Fig. 5 shows the ATR-FTIR spectra were acquired for pure GC and its solutions of KF (0.21 M) and saturated KF, K_2CO_3 and K_3PO_4. The main peaks attribution is reported in Table 2.

The addition of KF, K_2CO_3 and K_3PO_4 induced a shift to lower wavenumbers in the –OH stretching band [12,19]. This finding was particularly clear in the case of potassium fluoride and was related to the weakening of the –OH stretching due to the interaction of GC with the anion. For KF this behavior was found to be concentration-dependent [19]. However, the presence of salt did not significantly alter the position of the C-H stretching modes signals that fall in the range between 2875 and 2990 cm^{-1}. Interestingly, in the presence of saturated KF a remarkable shift of the C=O stretching band from 1763 to 1790 cm^{-1} was observed. These data seem to suggest that potassium fluoride ion pairs are intercalated between two GC molecules, thus perturbing the hydrogen bond between the carbonyl moiety and the –OH group. As a consequence, the ion–dipole C=O···K$^+$ interaction becomes weaker than the pristine HB, and the C=O stretching band shifts to a higher wavenumber [19]. Such marked effect was not detected in the case of K_2CO_3 and K_3PO_4 that showed a reduced influence on GC intermolecular HB compared to KF, as it was also confirmed by the O-H stretching band shift. For this reason, the position of the C=O stretching signal remained substantially unchanged.

Fig. 6 shows the ATR-FTIR spectra of CDCl$_3$ and GC in CDCl$_3$ between 4000 and 500 cm^{-1}.

The FTIR spectrum of CDCl$_3$ shows two characteristic peaks located at 2250 cm^{-1} and 912 cm^{-1} that were attributed to the C-D [56] and C-Cl stretching modes, respectively. When GC is dissolved in CDCl$_3$ the –OH stretching band exhibits a maximum at 3421 cm^{-1}, with no remarkable shift with respect to the pure liquid (see Table 2). Interestingly, for the C=O stretching signal the peak maximum was shifted towards higher wavenumbers, from 1763 to 1792 cm^{-1}. This effect can could be related to the ability of CDCl$_3$ to form hydrogen bonds [57,58].

The interaction between the GC carboxyl group and deuterium is weaker than the pristine C = O···H interaction between two GC
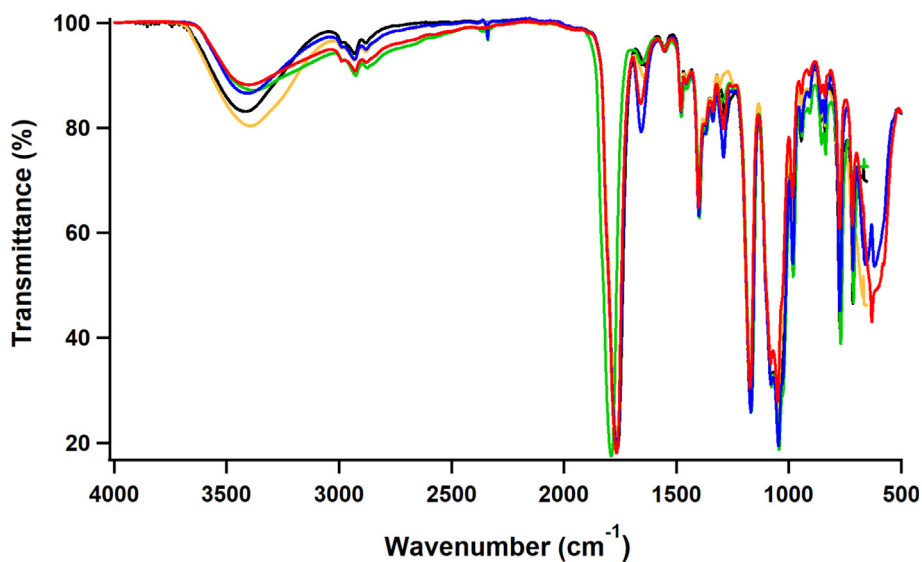
Fig. 5. ATR-FTIR spectra of pure GC (black), KF 0.21 M (orange) in GC, and saturated solutions of KF (green), K_2CO_3 (blue) and K_3PO_4 (red) in GC.

Table 2
Main peaks in the ATR-FTIR and NIR spectra run on pure GC, KF 0.21 M in GC, and saturated solutions of KF, K_2CO_3 and K_3PO_4 in GC.

|	ATR-FTIR			NIR		
	O-H stretch	C-H stretch	C = O stretch	O-H 1st overtone	C-H 1st overtone	C = O 2nd overtone
Pure GC	3420	2990 2931 2881	1763	6966	6009 5867 5685	5245
KF 0.21M	3389	2990 2932 2881	1763	6974	6009 5865 5683	5226
Saturated KF	3370	2987 2927 2875	1790	6981	6009 5865 5685	5236
Saturated K_2CO_3	3409	2988 2929 2879	1765	6971	6009 5863 5683	5226
Saturated K_3PO_4	3398	2987 2925 2875	1767	6970	6011 5863 5685	5246
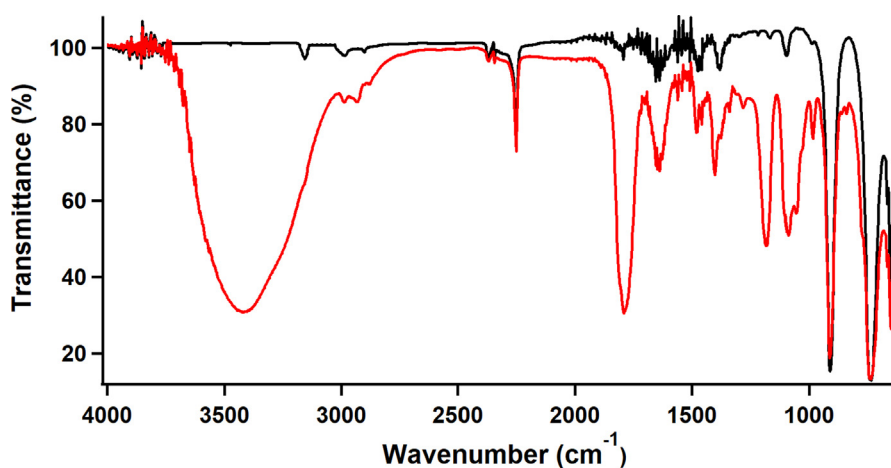
Fig. 6. ATR-FTIR spectra of $CDCl_3$ (black) and GC in $CDCl_3$ (red).

molecules. This results in a strengthening of the C = O bond, with a consequent peak shift to higher wavenumbers.

The NIR spectra showed a set of different new peaks in the regions between 7200 and 6100 cm^{-1}, 6000 and 5400 cm^{-1} and

5300 and 5000 cm^{-1} (see Fig. 7). The first of these peaks is mainly due to the first overtone stretching for –OH groups. The peak around 6966 cm^{-1} for pure GC is assigned to an –OH first overtone stretching vibration involved in an intermolecular hydrogen bond-
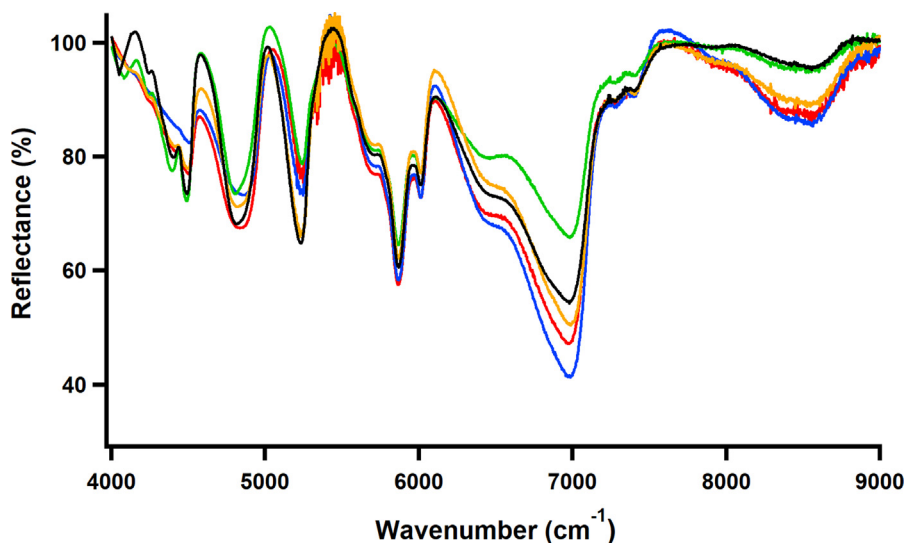
Fig. 7. NIR spectra of pure GC (black), KF 0.21 M (orange) in GC, and saturated solutions of KF (green), K_2CO_3 (blue) and K_3PO_4 (red) in GC.

ing. It was shifted to 6981 cm^{-1} for the saturated solution of KF in GC and to intermediate values for the other samples investigated (see Table 2). The second set of signals, that exhibits three main contributions approximately at 6010, 5865 and 5683 cm^{-1}, is assigned to the first overtone of the C-H stretching. As observed in ATR-FTIR spectra, the addition of the different salts did not result in a wavenumber shift. The third spectral region of interest (5300–5000 cm^{-1}) showed a definite band centered around 5230 cm^{-1} and is assigned to the second overtone of the C=O stretching.

The additional peaks observed in the range between 5000 and 4000 cm^{-1} are assigned to a combination of C=O, O-H, and C-H stretching [59].

Following the studies of Czarnecki and coworkers on the self-association of butyl alcohols in the pure liquid phase [60,61] the band due to –OH group in the region 7200 – 6100 cm^{-1} was deconvoluted into a sum of Gaussian profiles, and the different contributions were attributed to different types of –OH bond. The deconvoluted spectrum of pure GC is shown in Fig. 8 as an example of the fitting procedure, and the main results obtained for all the investigated samples are reported in Table 3.

The deconvolution of the NIR spectra identified four different peaks, centered at ~6420, ~6760, ~6930 and ~7035 cm^{-1}. The signal at higher wavenumber (peak δ, around 7035 cm^{-1}) was attributed to the first overtone of –OH stretching modes in the GC monomer. The addition of the different salts did not affect the position and the relative area of the peak, suggesting that the presence of the electrolytes did not alter the fraction of free GC monomers. Interestingly, this fraction is not predominant among the four different contributions, meaning that a strong association occurs between

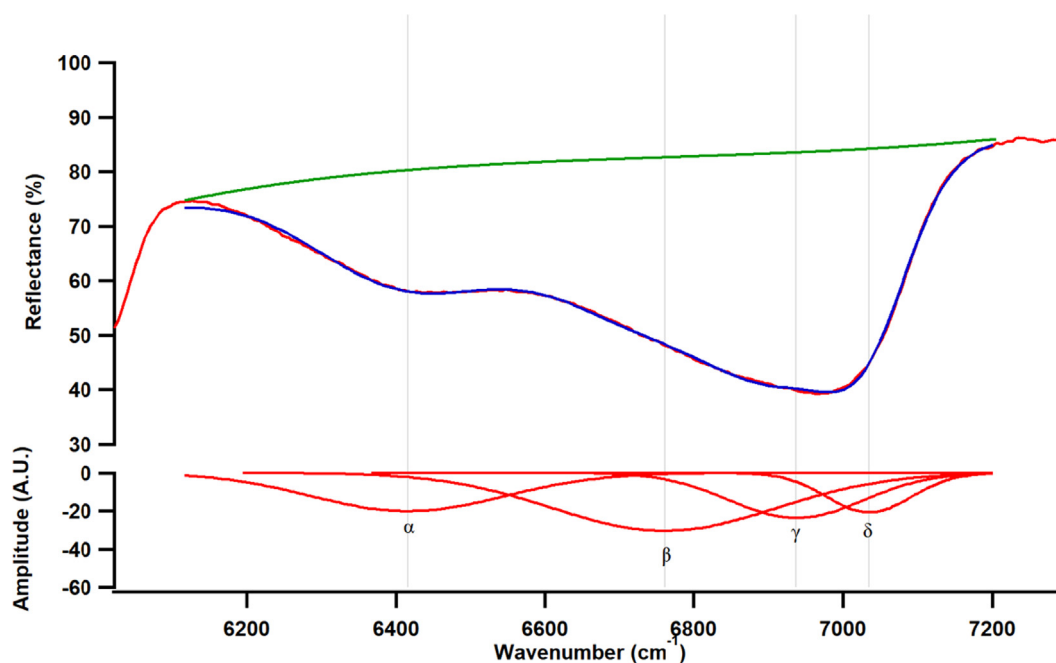**Fig. 8.** Top: experimental NIR spectra of pure GC (red) and the best fit after the deconvolution procedure (blue) in the range 7200–6100 cm^{-1}. Bottom: the separated deconvoluted peaks corresponding to the different contributions to the –OH band.

Table 3
Peak position (cm^{-1}) and relative area (%) obtained from the deconvolution of the OH band in the 7200–6100 cm^{-1} region.

	Peak α		Peak β		Peak γ		Peak δ	
	Position (cm^{-1})	Area (%)	Position (cm^{-1})	Area (%)	Position (cm^{-1})	Area (%)	Position (cm^{-1})	Area (%)
Pure GC	6416	24.8	6760	43.8	6937	20.2	7035	11.2
KF 0.21M	6417	28.2	6761	37.8	6933	20.7	7038	13.3
Saturated KF	6425	37.0	6770	31.7	6930	18.8	7031	12.5
Saturated K$_2$CO$_3$	6412	30.2	6751	37.3	6931	20.4	7037	12.2
Saturated K$_3$PO$_4$	6405	30.5	6748	37.5	6927	20.1	7031	12.0

GC molecules even in the absence of salts and that free GC molecules represents a relatively small fraction of the overall liquid. These results are in good agreement with the experimental data reported in the case of concentrated alcohol solutions, where the hydrogen-bonded associated structures are the dominating components [62].

According to the band assignment proposed by Czarnecki *et al.* [60,61] the peak located around 6930 cm^{-1} (peak γ) could be assigned to the free terminal –OH groups in linear aggregates (see Fig. 2). Interestingly, this band could also be attributed to –OH stretching modes in cyclic GC dimers (see Fig. 3), that can be considered intermediate species between the monomers and more complex polymer-like aggregates. Generally, the bands due to –OH vibrations in open and cyclic aggregates of various length occur at lower wavenumber, e.g. around 6200–6600 cm^{-1} in the case of butyl alcohols.

Nevertheless, the high strain in small cyclic structures such as dimers may result in a weakening in the hydrogen bond and a consequent blue shift in the –OH absorption band, that occurs around 6800–6900 cm^{-1}.

The maximum of peak γ showed a decrease in the wavenumber upon the addiction of the different salts: the interaction between the anions and the hydroxyl moiety was able to weaken the O-H bond, resulting in a band shift towards lower wavenumbers. The relative area of the peak remained unaltered, with the exception of the sample containing GC and saturated KF, that shows a slight reduction from 20.2 to 18.8%. The peaks centered around 6420 and 6760 cm^{-1} (peak α and β respectively) could be ascribed to the –OH stretching modes in different GC aggregates of various length (both cyclic and linear) [60,61], and represented the major contributions in terms of relative areas. Peak α was related to the –OH stretching in linear aggregates, that occurs at lower wavenumbers, while peak β was attributed to the stretching of bent –OH bonds in cyclic structures, where the larger strain causes a shift towards higher wavenumbers. The trend of the relative areas was very interesting: as the concentration of KF increases, the area of peak α increases from 24.8 to 37.0%, while peak β shows a reduction from 43.8 to 31.7%. A similar trend was also observed for the samples containing saturated K$_2$CO$_3$ and K$_3$PO$_4$. These results suggested that the addition of salt can promote the formation of linear, elongated GC aggregates, with a significant reduction in the fraction of cyclic clusters.

The analysis of the temperature-induced spectral modifications provides a further confirmation of the proposed model for GC molecular association. NIR spectra of pure GC were recorded over a temperature range of 0 to 90 °C with steps of 10 °C. Fig. 9 shows the relative area (%) of the 4 different peaks (α, β, γ, δ) obtained from the deconvolution as a function of temperature. The spectra are reported in Figure S1 in the Supplementary Material.

As the temperature increases the area of peaks α and β shows a progressive decrease, which is more pronounced in the case of the latter component. The area of peaks γ and δ exhibits an opposite trend, increasing gradually at higher temperatures.

These results suggest that the temperature increase leads to the dissociation of the large linear and cyclic GC aggregates (peaks α and β) into dimers (peak γ) and monomers (peak δ). It is important to note that the predominant fraction is represented by oligomeric cyclic structures (peak β), even at high temperatures.

Linear aggregates, which are the second most abundant species at lower temperatures (peak α), showed the most pronounced temperature dependence, and became the minor contribution above 60 °C.
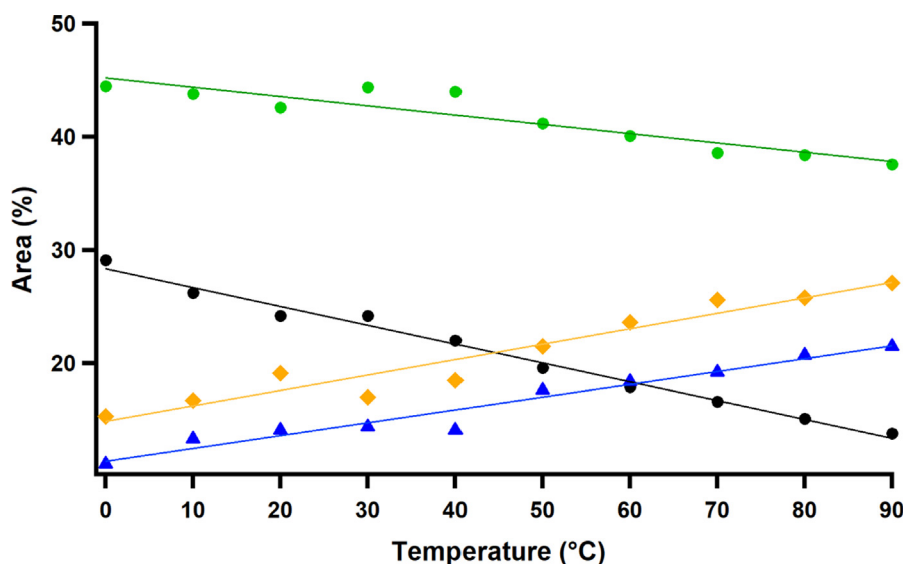
Fig. 9. Relative area (%) obtained from the deconvolution of the OH band in pure GC NIR spectrum for the peak α (black dots), β (green dots), γ (yellow diamonds) and δ (blue triangles) as a function of temperature. The solid lines represent the best linear regressions.
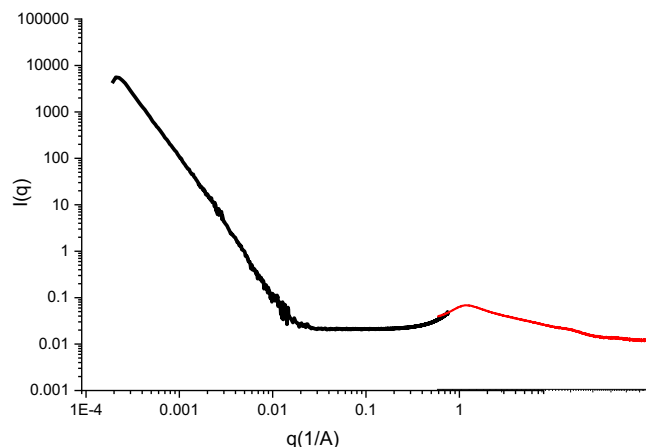
Fig. 10. SAXS-WAXS curves of pure GC solvent showing the total *q*-range covered by the combined techniques, i.e. between $3 \cdot 10^{-4}$ and 8.5 Å^{-1}. SAXS (black curve) and WAXS (red curve) of pure GC.

3.3. SAXS and WAXS

Scattering and diffraction experiments were carried out on samples containing pure glycerol carbonate and its solutions with the same salts studied by IR spectroscopy. The combined use of SAXS and WAXS allow to probe the structuring effect exerted by different solutes over a wide range of length scales, i.e. approximately 5 orders of magnitude, from angstroms to micrometers. The overall profile obtained for pure GC is shown in Fig. 10, where the overlap of SAXS and WAXS plots shows marked correlations at $q \geq 0.4$ Å^{-1}, (corresponding to distances shorter than 16 Å) and at low *q* values (~0.003 Å^{-1}, corresponding to ~ 2 μm), in agreement with the proposed association of GC monomers into dimers and long one-dimensional aggregates through hydrogen bonding. Short-range intermolecular non-covalent interactions produce a defined peak in the high *q* region of the scattering diagram (WAXS), while at longer distances correlations are looser and merely result in a shoulder or even just in a slope change (SAXS), as in the case of pure GC over long distances [63–65].

The SAXS patterns of the salt solutions in GC are shown in Fig. 11. All profiles present a slope change (crossover point), which becomes more evident in the case of saturated K$_2$CO$_3$, saturated KF

and KF 0.21 M indicating that in these systems stronger interactions span across hundreds of nanometers. As suggested by previous conductivity and rheology measurements, potassium fluoride and potassium carbonate form solvent-assisted ion pairs, intercalate between GC monomers and strengthen the structuredness of the pure solvent even at a supramolecular level [12,19]. These findings are well in line with the SAXS scattering profiles of the systems studied in this work. Specifically, the change in slope was fitted for the pure GC and for the saturated K$_3$PO$_4$ solution with a two-power law model (SasView User Documentation, https:// www.sasview.org/) (see Figure S2, S3 and Table S1 in the Supplementary Material). Such model describes the intensity *I*(*q*) combining the exponential *q*-decay with two exponents and a scaling coefficient. For the samples showing a shoulder, a correlation length model was used for the fitting procedure (see the Supplementary Material for the details about the model). Table S1 shows the parameters extracted from the fitting of the SAXS curves. Here the high-*q* term describes the Porod scattering from clusters, that could be generated by monomer–monomer interactions in the lateral direction, and the low-*q* term is a Lorentzian function which in macromolecular solutions accounts for the scattering of chains interacting with the solvent [66]. In the present systems this latter contribution could be a result of ion–dipole interactions from alternated GC-ions in the longitudinal direction, arranged in a short ribbon or in a cyclic configuration. The sample with KF 0.21 M shows the most prominent shoulder around 0.01 Å^{-1} which corresponds to a correlation length of 113 Å (Figure S4), whereas for saturated KF the shoulder is less pronounced and shifted to higher *q* values, with a shorter correlation length (88 Å) (Figure S5). The sample containing K$_2$CO$_3$ in GC at saturation shows a weak bump at lower *q*, giving a correlation length of 400 Å (see Figures 11 and S6, and Table S1).

The WAXS experiments covered the range between 0.7 A^{-1} and 8.5 Å^{-1} and indicated a rise in the intensity at high *q* beyond the detection limits of SAXS with a specific sequence: GC < K$_3$PO$_4$ < K$_2$-CO$_3$ < KF. In this range the scattered intensity of all samples shows a pronounced peak centered around the same values, while a marked narrowing was observed upon addition of the salt to the pure solvent (see Fig. 12). Such peaks can be ascribed to short-range ribbon interactions between GC and intercalated ion pairs, either in the lateral or in the longitudinal directions of the associated supramolecular structure [12,19]. The correlation peak in the
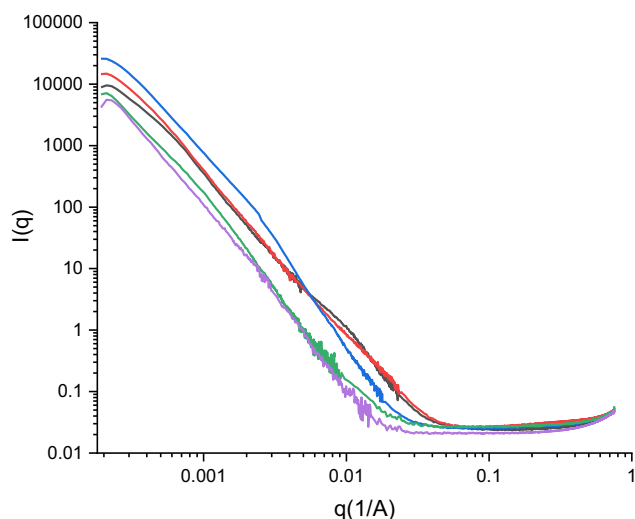
Fig. 11. Intensity SAXS plots of all five samples: pure GC (purple) KF 0.21 M (black); saturated KF (red); saturated K$_2$CO$_3$ (blue); saturated K$_3$PO$_4$ (green).
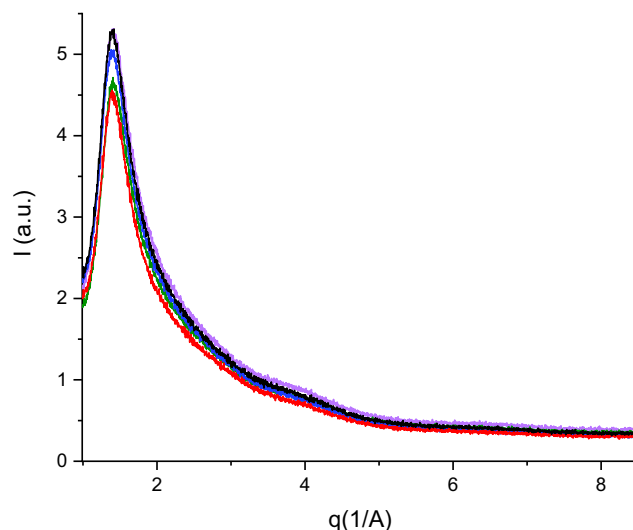
Fig. 12. WAXS plots for GC (purple) and the four salt mixtures KF 0.21 M (black); saturated KF (red); saturated K$_2$CO$_3$ (blue); saturated K$_3$PO$_4$ (green).

Table 4
Simulation parameters for the Lorentzian function.

Salt	Area Fit	Center Max ($Å^{-1}$)	Max Height (a.u.)	FWHM
Pure GC	4.7	1.418	5.3	0.6
KF 0.21M	4.6	1.4	5.28	0.59
Saturated KF	3.2	1.39	4.48	0.49
Saturated K_2CO_3	4	1.39	5	0.54
Saturated K_3PO_4	3.4	1.405	4.68	0.5

WAXS region was modelled for all samples with a built-in Lorentzian function from OriginPro software (see Figure S2 in the Supplementary Material), and the simulation parameters are listed in Table 4. In particular, we decided to reproduce the left, low-q side of the peak, and neglect the pronounced asymmetry arising from other contributions that occur over shorter distances and can be hardly identified without ambiguity. This was done in order to avoid possible over-interpretation of the data that would be introduced by convoluting more than one distribution.

From the Full Width at Half Maximum (FWHM) values we can obtain information on the extension of the coherence domains, that is the space extent along which the interactions are established and propagated. These domains are inversely proportional to the FWHM [67]. The results indicate that the coherence domains are more extended in the case of the saturated solution of KF in GC. Thus, in this system the persistence length due to extended HB networks is larger.

The results reported in this work confirm the presence of supramolecular structures both in pure GC and in the presence of basic anions. In addition, SAXS profiles indicate for each system a correlation length value over which the interactions take place.

The efficacy of the investigated salts on the structuring of GC followed a trend where fluoride was the most effective and phosphate the least efficient in strengthening the liquid structure: K_3PO_4 < K_2CO_3 < KF. This observation, that agrees with previous findings [12] may be justified by considering i) the different delocalization of the charge in the three anions (i.e. their polarizability); ii) their different basicity; and iii) the match between the different anion geometry and the hydrogen bond directionality [68]. In fact in the small fluoride ion the charge is completely localized around the nucleus, its polarizability is among the lowest values known, and therefore can play a powerful role as HB acceptor in the presence of a donor group such as an –OH residue. On the other hand, F^- is spherical and can interact directly with the –OH group. Instead, carbonate is trigonal planar and phosphate is tetrahedral, their O$^{...}$H interaction is not aligned with the H-O bond in GC, and therefore the interaction is weaker than with KF, although phosphate and carbonate bear a three and two negative charges, respectively.

4. Conclusion

Near-infrared and attenuated total reflection Fourier-transform infrared spectroscopy, small- and wide-angle X-ray scattering experiments were performed on pure liquid glycerol carbonate and on its solutions of saturated KF, K_2CO_3, K_3PO_4 in order to probe the structure of the solvent. The choice of these salts is based on previous results that suggested their capacity to strengthen the structure of GC.

This work confirms the presence of clusters in the samples that justify the experimental results. The observed structures are held together by hydrogen bonds between the carbonyl and the hydroxyl moieties of the GC molecules and by van der Waals interactions. By these we mean the totality of cooperative many body fluctuation interactions from microwave, infrared, visible and UV contributions. The contributions from cooperative dipolar interactions are particularly strong because of the large molecular dipole moment.

The singularly strong consistency of liquid GC compared to that of water and of other organic cyclic carbonates (ethylene carbonate and propylene carbonate) reflects in its physico-chemical properties (e.g. Trouton's constant) and peculiar behaviors (e.g. rheology, thixotropy, glass transition). Given the presence in GC of an HB acceptor and donor, multiple options are available for the formation of a rich variety of dynamic transient associated structures: single dimers, ribbon-like monodimensional structures, and also bidimensional sheets. Salts containing an anion that can efficiently act as HB acceptor (fluoride, carbonate and phosphate), are able to stabilize the supramolecular clusters by interacting directly with the –OH end group of GC. Interestingly, the monovalent fluoride seems to be most effective, while the trivalent phosphate is the least efficient in structuring the solvent. This observation may be explained by considering i) the different delocalization of the charge in the three anions and therefore their polarizability; ii) their different basicity and HB accepting capacity and iii) their different geometry. One should expect that phosphate, bearing three net charges, should be able to tighten the structure of GC more than the divalent carbonate and the monovalent fluoride. Instead, the structuring effect of the anion on GC goes the opposite way. This evidence suggests that the most important features are the better accepting capacity and the possibility of linear geometry.

CRediT authorship contribution statement

Duccio Tatini: Conceptualization, Data curation, Investigation, Methodology, Writing - original draft, Writing - review & editing. **Ilaria Clemente:** Data curation, Investigation, Formal analysis, Writing - original draft. **Moira Ambrosi:** Validation, Visualization. **Sandra Ristori:** Conceptualization, Formal analysis, Investigation, Writing - original draft, Writing - review & editing. **Barry W. Ninham:** Writing - original draft. **Pierandrea Lo Nostro:** Conceptualization, Investigation, Supervision, Writing - original draft, Writing - review & editing.

Declaration of Competing Interest

The authors declare that they have no known competing financial interests or personal relationships that could have appeared to influence the work reported in this paper.

Acknowledgement

Appendix A. Supplementary material

Supplementary data to this article can be found online at https://doi.org/10.1016/j.molliq.2021.116413.

References

[1] H. Wang, X. Pu, The structure and properties of a novel hydroxyl-terminated hyperbranched polymer for inhibiting shale hydration, Chemistry Select. 4 (2019) 11239–11246, https://doi.org/10.1002/slct.201902524.

[2] P. de Caro, M. Bandres, M. Urrutigoïty, C. Cecutti, S. Thiebaud-Roux, Recent progress in synthesis of glycerol carbonate and evaluation of its plasticizing properties, Front. Chem. 7 (2019), https://doi.org/10.3389/fchem.2019.00308.

[3] M.A. Rasool, P.P. Pescarmona, I.F.J. Vankelecom, Applicability of organic carbonates as green solvents for membrane preparation, ACS Sustain. Chem. Eng. 7 (2019) 13774–13785, https://doi.org/10.1021/acssuschemeng.9b01507.

[4] Y. Ji, Recent development of heterogeneous catalysis in the transesterification of glycerol to glycerol carbonate, Catalysts. 9 (2019) 581, https://doi.org/10.3390/catal9070581.

[5] S. Nomanbhay, M.Y. Ong, K.W. Chew, P.-L. Show, M.K. Lam, W.-H. Chen, Organic carbonate production utilizing crude glycerol derived as by-product of biodiesel production: a review, Energies. 13 (2020) 1483, https://doi.org/10.3390/en13061483.

[6] A. Zanoni, G. Gardoni, M. Sponchioni, D. Moscatelli, Valorisation of glycerol and CO2 to produce biodegradable polymer nanoparticles with a high percentage of bio-based components, J. CO2 Util. 40 (2020), https://doi.org/10.1016/j.jcou.2020.101192 101192.

[7] H. Zhang, H. Li, A. Wang, C. (Charles) Xu, S. Yang, Progress of Catalytic Valorization of Bio-Glycerol with Urea into Glycerol Carbonate as a Monomer for Polymeric Materials, Adv. Polym. Technol. 2020 (2020) 7207068. https://doi.org/10.1155/2020/7207068.

[8] F. Boujioui, H. Damerow, F. Zhuge, J.-F. Gohy, Solid polymer electrolytes based on copolymers of cyclic carbonate acrylate and n-butylacrylate, Macromol. Chem. Phys. 221 (2020) 1900556, https://doi.org/10.1002/macp.201900556.

[9] S. Kotanen, T. Laaksonen, E. Sarlin, Feasibility of polyamines and cyclic carbonate terminated prepolymers in polyurethane/polyhydroxyurethane synthesis, Mater. Today Commun. 23 (2020), https://doi.org/10.1016/j.mtcomm.2019.100863 100863.

[10] E. Hernández, R. Santiago, C. Moya, P. Navarro, J. Palomar, Multiscale evaluation of CO2-derived cyclic carbonates to separate hydrocarbons: Drafting new competitive processes, Fuel Process. Technol. 212 (2021), https://doi.org/10.1016/j.fuproc.2020.106639 106639.

[11] S. Sahani, S.N. Upadhyay, Y.C. Sharma, Critical review on production of glycerol carbonate from byproduct glycerol through transesterification, Ind. Eng. Chem. Res. 60 (2021) 67–88, https://doi.org/10.1021/acs.iecr.0c05011.

[12] F. Sarri, D. Tatini, D. Tanini, M. Simonelli, M. Ambrosi, B.W. Ninham, A. Capperucci, L. Dei, P. Lo Nostro, Specific ion effects in non-aqueous solvents: The case of glycerol carbonate, J. Mol. Liq. 266 (2018) 711–717, https://doi.org/10.1016/j.molliq.2018.06.120.

[13] Y. Chernyak, Dielectric constant, dipole moment, and solubility parameters of some cyclic acid esters, J. Chem. Eng. Data. 51 (2006) 416–418, https://doi.org/10.1021/je050341y.

[14] M.O. Sonnati, S. Amigoni, E.P.T. de Givenchy, T. Darmanin, O. Choulet, F. Guittard, Glycerol carbonate as a versatile building block for tomorrow: synthesis, reactivity, properties and applications, Green Chem. 15 (2013) 283–306, https://doi.org/10.1039/C2GC36525A.

[15] R. Bosque, J. Sales, Polarizabilities of solvents from the chemical composition, J. Chem. Inf. Comput. Sci. 42 (2002) 1154–1163, https://doi.org/10.1021/ci025528x.

[16] Y. Chernyak, J.H. Clements, Vapor pressure and liquid heat capacity of alkylene carbonates, J. Chem. Eng. Data. 49 (2004) 1180–1184, https://doi.org/10.1021/je034173q.

[17] N. Peruzzi, B.W. Ninham, P. Lo Nostro, P. Baglioni, Hofmeister phenomena in nonaqueous media: the solubility of electrolytes in ethylene carbonate, J. Phys. Chem. B. 116 (2012) 14398–14405, https://doi.org/10.1021/jp309157x.

[18] N. Peruzzi, P. Lo Nostro, B.W. Ninham, P. Baglioni, The solvation of anions in propylene carbonate, J. Solut. Chem. 44 (2015) 1224–1239, https://doi.org/10.1007/s10953-015-0335-z.

[19] F. Sarri, D. Tatini, M. Ambrosi, E. Carretti, B.W. Ninham, L. Dei, P. Lo Nostro, The curious effect of potassium fluoride on glycerol carbonate. How salts can influence the structuredness of organic solvents, J. Mol. Liq. 255 (2018) 397–405, https://doi.org/10.1016/j.molliq.2018.01.152.

[20] B.W. Ninham, P. Lo Nostro, Molecular Forces and Self Assembly, in: Colloid, Nano Sciences and Biology, Cambridge University Press, Cambridge, 2010, https://doi.org/10.1017/CBO9780511811531.

[21] S.T. Hyde, Aqua reticulata: topology of liquid water networks, in: Aqua Incogn. Why Ice Floats Water Galileo 400 Years On, Connor Court Publishing, Ballarat, 2014: pp. 145–175. https://www.connorcourtpublishing.com.au/Aqua-Incognita-Why-Ice-Floats-on-Water-and-Galileo-400-Years-On–Pierandrea-Lo-Nostro-and-Barry-Ninham-_p_327.html.

[22] Y.M. Delavoux, M. Gilmore, M.P. Atkins, M. Swadźba-Kwaśny, J.D. Holbrey, Intermolecular structure and hydrogen-bonding in liquid 1,2-propylene carbonate and 1,2-glycerol carbonate determined by neutron scattering, Phys. Chem. Chem. Phys. 19 (2017) 2867–2876, https://doi.org/10.1039/C6CP07790K.

[23] A.E. Eisenhart, T.L. Beck, Quantum simulations of hydrogen bonding effects in glycerol carbonate electrolyte solutions, J. Phys. Chem. B. 125 (2021) 2157–2166, https://doi.org/10.1021/acs.jpcb.0c10942.

[24] H. Yamatera, B. Fitzpatrick, G. Gordon, Near infrared spectra of water and aqueous solutions, J. Mol. Spectrosc. 14 (1964) 268–278, https://doi.org/10.1016/0022-2852(64)90121-3.

[25] J. Muncan, R. Tsenkova, Aquaphotomics—From Innovative Knowledge to Integrative Platform in Science and Technology, Molecules 24 (2019) 2742, https://doi.org/10.3390/molecules24152742.

[26] E.B. van de Kraats, J. Munćan, R.N. Tsenkova, Aquaphotomics – Origin, concept, applications and future perspectives, Substantia. 3 (2019) 13–28. https://doi.org/10.13128/Substantia-702.

[27] K.B. Beć, J. Grabska, C.W. Huck, Near-infrared spectroscopy in bio-applications, Molecules 25 (2020) 2948, https://doi.org/10.3390/molecules25122948.

[28] Q. Dong, C. Yu, L. Li, L. Nie, D. Li, H. Zang, Near-infrared spectroscopic study of molecular interaction in ethanol-water mixtures, Spectrochim. Acta. A. Mol. Biomol. Spectrosc. 222 (2019), https://doi.org/10.1016/j.saa.2019.117183 117183.

[29] A.N. Fletcher, C.A. Heller, Self-association of alcohols in nonpolar solvents, J. Phys. Chem. 71 (1967) 3742–3756, https://doi.org/10.1021/j100871a005.

[30] L. Stordrange, A.A. Christy, O.M. Kvalheim, H. Shen, Y. Liang, Study of the self-association of alcohols by near-infrared spectroscopy and multivariate 2D techniques, J. Phys. Chem. A. 106 (2002) 8543–8553, https://doi.org/10.1021/jp013670f.

[31] M. Ambrosi, P.L. Nostro, E. Fratini, L. Giustini, B.W. Ninham, P. Baglioni, Effect of headgroup chirality in nanoassemblies. Part 1. Self-assembly of d-isoascorbic acid derivatives in water, J. Phys. Chem. B. 113 (2009) 1404–1412, https://doi.org/10.1021/jp8092644.

[32] Y. Mikami, A. Ikehata, C. Hashimoto, Y. Ozaki, Near-Infrared (NIR) study of hydrogen bonding of methanol molecules in polar and nonpolar solvents: an approach from concentration-dependent molar absorptivity, Appl. Spectrosc. 68 (2014) 1181–1189, https://doi.org/10.1366/14-07449.

[33] M. Kwaśniewicz, M.A. Czarnecki, The effect of chain length on mid-infrared and near-infrared spectra of aliphatic 1-alcohols, Appl. Spectrosc. 72 (2018) 288–296, https://doi.org/10.1177/0003702817732253.

[34] J. Dong, Y. Ozaki, K. Nakashima, Infrared, Raman, and near-infrared spectroscopic evidence for the coexistence of various hydrogen-bond forms in poly(acrylic acid), Macromolecules 30 (1997) 1111–1117, https://doi.org/10.1021/ma960693x.

[35] H. Büning-Pfaue, Analysis of water in food by near infrared spectroscopy, Food Chem. 82 (2003) 107–115, https://doi.org/10.1016/S0308-8146(02)00583-6.

[36] G.X. Zhou, Z. Ge, J. Dorwart, B. Izzo, J. Kukura, G. Bicker, J. Wyvratt, Determination and differentiation of surface and bound water in drug substances by near infrared spectroscopy, J. Pharm. Sci. 92 (2003) 1058–1065, https://doi.org/10.1002/jps.10375.

[37] O. Glatter, O. Kratky, Small Angle X-ray Scattering, Academica Press, New York, 1982.

[38] M.-H. Ropers, G. Brezesinski, Lipid ordering in planar 2D and 3D model membranes, Soft Matter 9 (2013) 9440–9448, https://doi.org/10.1039/C3SM51582F.

[39] J. Defebvin, S. Barrau, G. Stoclet, C. Rochas, J.-M. Lefebvre, In situ SAXS/WAXS investigation of the structural evolution of poly(vinylidene fluoride) upon uniaxial stretching, Polymer 84 (2016) 148–157, https://doi.org/10.1016/j.polymer.2015.12.041.

[40] V. Kamysbayev, V. Srivastava, N.B. Ludwig, O.J. Borkiewicz, H. Zhang, J. Ilavsky, B. Lee, K.W. Chapman, S. Vaikuntanathan, D.V. Talapin, Nanocrystals in molten salts and ionic liquids: experimental observation of ionic correlations extending beyond the Debye length, ACS Nano 13 (2019) 5760–5770, https://doi.org/10.1021/acsnano.9b01292.

[41] T.L. Greaves, D.F. Kennedy, S.T. Mudie, C.J. Drummond, Diversity Observed in the Nanostructure of Protic Ionic Liquids, J. Phys. Chem. B. 114 (2010) 10022–10031, https://doi.org/10.1021/jp103863z.

[42] J. Pepin, V. Gaucher, C. Rochas, J.-M. Lefebvre, In-situ SAXS/WAXS investigations of the mechanically-induced phase transitions in semi-crystalline polyamides, Polymer 175 (2019) 87–98, https://doi.org/10.1016/j.polymer.2019.04.073.

[43] P. Boesecke, Reduction of two-dimensional small- and wide-angle X-ray scattering data, J. Appl. Crystallogr. 40 (2007) s423–s427, https://doi.org/10.1107/S0021889807001100.

[44] T. Narayanan, M. Sztucki, P. Van Vaerenbergh, J. Léonardon, J. Gorini, L. Claustre, F. Sever, J. Morse, P. Boesecke, A multipurpose instrument for time-resolved ultra-small-angle and coherent X-ray scattering, J. Appl. Crystallogr. 51 (2018) 1511–1524, https://doi.org/10.1107/S1600576718012748.

[45] H.P. Bennetto, E.F. Caldin, Solvent effects on the kinetics of the reactions of nickel(II) and cobalt(II) ions with 2,2′-bipyridyl and 2,2′,2″-terpyridyl, J. Chem. Soc. Inorg. Phys. Theor. (1971) 2191–2198, https://doi.org/10.1039/J19710002191.

[46] J.-Q. Dong, R.-S. Lin, W.-H. Yen, Heats of vaporization and gaseous molar heat capacities of ethanol and the binary mixture of ethanol and benzene, Can. J. Chem. (1988) 783–790, https://doi.org/10.1139/v88-136.

[47] Y. Marcus, The structuredness of solvents, J. Solut. Chem. 21 (1992) 1217–1230, https://doi.org/10.1007/BF00667218.

[48] Y. Marcus, The structuredness of water at elevated temperatures along the saturation line, J. Mol. Liq. 79 (1999) 151–165, https://doi.org/10.1016/S0167-7322(98)00109-3.

[49] R.M. Stephenson, ed., Handbook of the Thermodynamics of Organic Compounds, Springer Netherlands, Dordrecht, 1987. https://doi.org/10.1007/978-94-009-3173-2.

[50] W.J. Peppel, Preparation and properties of the alkylene carbonates, Ind. Eng. Chem. 50 (1958) 767–770, https://doi.org/10.1021/ie50581a030.

[51] Y. Marcus, Ions in Solution and their Solvation, John Wiley & Sons, Inc., Hoboken, New Jersey, 2015. https://www.wiley.com/en-us/Ions+in+Solution +and+their+Solvation-p-9781118892336 (accessed April 19, 2021).

[52] S.P. Verevkin, A.V. Toktonov, Y. Chernyak, B. Schäffner, A. Börner, Vapour pressure and enthalpy of vaporization of cyclic alkylene carbonates, Fluid Phase Equilib. 268 (2008) 1–6, https://doi.org/10.1016/j.fluid.2008.03.013.

[53] Y. Marcus, Effect of ions on the structure of water: structure making and breaking, Chem. Rev. 109 (2009) 1346–1370, https://doi.org/10.1021/cr8003828.

[54] Y.H. Zhao, M.H. Abraham, A.M. Zissimos, Determination of McGowan volumes for ions and correlation with van der waals volumes, J. Chem. Inf. Comput. Sci. 43 (2003) 1848–1854, https://doi.org/10.1021/ci0341114.

[55] Y. Marcus, Ion Solvation, Wiley, Chichester, 1985.

[56] C.S. Kinnaman, M.E. Cremeens, F.E. Romesberg, S.A. Corcelli, Infrared line shape of an α-carbon deuterium-labeled amino acid, J. Am. Chem. Soc. 128 (2006) 13334–13335, https://doi.org/10.1021/ja064468z.

[57] D.C. Daniel, J.L. McHale, Hydrogen bonding in CHCl3/DMSO-d6 and CDCl3/DMSO-h6 mixtures, J. Phys. Chem. A. 101 (1997) 3070–3077, https://doi.org/10.1021/jp9623507.

[58] N. Goutev, H. Matsuura, Hydrogen bonding in chloroform solutions of ethylenedioxy ethers. Spectroscopic evidence of bifurcated hydrogen bonds, J. Phys. Chem. A. 105 (2001) 4741–4748, https://doi.org/10.1021/jp004542e.

[59] H. Liu, B. Xiang, L. Qu, Structure analysis of ascorbic acid using near-infrared spectroscopy and generalized two-dimensional correlation spectroscopy, J. Mol. Struct. 794 (2006) 12–17, https://doi.org/10.1016/j.molstruc.2006.01.028.

[60] M.A. Czarnecki, H. Maeda, Y. Ozaki, M. Suzuki, M. Iwahashi, Resolution enhancement and band assignments for the first overtone of OH stretching mode of butanols by two-dimensional near-infrared correlation spectroscopy. Part I: sec-Butanol, Appl. Spectrosc. 52 (1998) 994–1000, https://doi.org/10.1366/0003702981944643.

[61] M.A. Czarnecki, H. Maeda, Y. Ozaki, M. Suzuki, M. Iwahashi, Resolution enhancement and band assignments for the first overtone of OH stretching modes of butanols by two-dimensional near-infrared correlation spectroscopy. 2. Thermal dynamics of hydrogen bonding in n- and tert-butyl alcohol in the pure liquid states, J. Phys. Chem. A. 102 (1998) 9117–9123, https://doi.org/10.1021/jp9823704.

[62] Y. Sun, X. Cui, W. Cai, X. Shao, Understanding the complexity of the structures in alcohol solutions by temperature–dependent near–infrared spectroscopy, Spectrochim. Acta. A. Mol. Biomol. Spectrosc. 229 (2020), https://doi.org/10.1016/j.saa.2019.117864 117864.

[63] J. Teixeira, Small-angle scattering by fractal systems, J. Appl. Crystallogr. 21 (1988) 781–785, https://doi.org/10.1107/S0021889888000263.

[64] F. Sedlmeier, D. Horinek, R.R. Netz, Spatial correlations of density and structural fluctuations in liquid water: A comparative simulation study, J. Am. Chem. Soc. 133 (2011) 1391–1398, https://doi.org/10.1021/ja1064137.

[65] H. Weiss, J. Mars, H. Li, G. Kircher, O. Ivanova, A. Feoktystov, O. Soltwedel, M. Bier, M. Mezger, Mesoscopic correlation functions in heterogeneous ionic liquids, J. Phys. Chem. B. 121 (2017) 620–629, https://doi.org/10.1021/acs.jpcb.6b11220.

[66] B. Hammouda, D.L. Ho, S. Kline, Insight into clustering in poly(ethylene oxide) solutions, Macromolecules 37 (2004) 6932–6937, https://doi.org/10.1021/ma049623d.

[67] B.E. Warren, X-Ray Diffraction, Illustrated edition, Dover Publications, New York, 1990.

[68] A. Shahi, E. Arunan, Why are hydrogen bonds directional?, J. Chem. Sci. 128 (2016) 1571–1577, https://doi.org/10.1007/s12039-016-1156-3.